Weak Topological Insulators and Composite Weyl Semimetals: β-Bi_{4}X_{4} (X=Br, I)

Cheng-Cheng Liu, Jin-Jian Zhou, Yugui Yao, and Fan Zhang

Weak Topological Insulators and Composite Weyl Semimetals: β-Bi$_4$X$_4$ (X=Br, I)

Cheng-Cheng Liu,[1, 2] Jin-Jian Zhou,[2] Yugui Yao,[2, *] and Fan Zhang[1, †]

[1]*Department of Physics, University of Texas at Dallas, Richardson, Texas 75080, USA*
[2]*School of Physics, Beijing Institute of Technology, Beijing 100081, China*

While strong topological insulators (STI) have been experimentally realized soon after their theoretical predictions, a weak topological insulator (WTI) has yet to be unambiguously confirmed. A major obstacle is the lack of distinct natural cleavage surfaces to test the surface selective hallmark of WTI. With a new scheme, we discover that β-Bi$_4$X$_4$ (X=Br, I), dynamically stable or synthesized before, can be prototype WTI with two natural cleavage surfaces, where two anisotropic Dirac cones stabilize and annihilate, respectively. We further find four surface-state Lifshitz transitions under charge doping and two bulk topological phase transitions under uniaxial strain. Near the WTI-STI transition, there emerges a novel Weyl semimetal phase, in which the Fermi arcs generically appear at both cleavage surfaces whereas the Fermi circle only appears at one selected surface.

Introduction.—The discovery of topological insulators [1–3] has led to an ongoing revolution deepening our fundamental understanding of quantum materials. The controllable bulk topological quantum phase transitions and the protected spin-momentum locked surface states may ultimately lead to unprecedented advances in technologies, e.g., the Majorana-based fault-tolerant quantum computing [4]. Historically, strong and weak topological insulators (STI and WTI) were predicted together, characterized by four Z_2 invariants $(\nu_0; \nu_1 \nu_2 \nu_3)$ [5–7]. A STI has a nontrivial ν_0 index, whereas a WTI with vanishing ν_0 has nontrivial $(\nu_1 \nu_2 \nu_3)$ indices, and consequently they have odd and even number of Dirac surface states, respectively [5]. Astonishingly, STI are not at all rare in nature. Over a dozen documented materials have been identified [8–14] as STI under readily accessible experimental conditions. Notably, their lateral structure offers a superior advantage to observe the hallmark of STI, a surface Dirac cone, without intended surface passivation that could be challenging. However, the unambiguous experimental confirmation of WTI is still elusive [14].

Thus far there have been two routes to construct WTI, i.e., to stack weakly coupled layers [15–17] of quantum spin Hall insulators (QSHI), or to engineer a superlattice [18, 19] of alternating layers with multiple band inversions. Evidently, these designer WTI pose extreme experimental challenges. In the first route, the protected surface metallicity will only be present at non-cleavage surfaces (non-parallel to the layers), yet surface roughness and dangling bonds would prevent us from observing this hallmark [16]. In the second route, though the surface states can survive at the cleavage surface (parallel to the layers), the intra- and inter-layer couplings within a supercell must be fine tuned in material synthesis. Therefore, to unambiguously determine the existence of WTI and to explore the exotic phenomena uniquely hosted by WTI, it is crucial to develop a new route.

Here we propose to realize the WTI in a van der Waals (vdW) material that is a periodic stack of 1D atomic chains. Such a WTI possesses two natural cleavage planes, enabling respective observations of stabilization and annihilation of distinct surface Dirac cones. We discover that β-Bi$_4$X$_4$ (X=I, Br) can be such a class of WTI. Markedly, with a chemical formula as simple as the prototype STI Bi$_2$X$_3$ (X=Se, Te), β-Bi$_4$X$_4$ are real crystalline solids rather than artificial periodic heterostructures. β-Bi$_4$I$_4$ has been successfully grown as a large crystal before [20–23], and β-Bi$_4$Br$_4$ is demonstrated to be similarly stable [24]. After revealing their unique crystal structure, topological band properties, and surface Lifshitz transitions, we further examine their topological phase transitions under uniaxial strain. Intriguingly, a novel Weyl semimetal (WSM) phase emerges near the WTI-STI transition; in addition to the existence of Fermi arcs at both cleavage surfaces as the case of WSM, a Fermi circle only exists at one selected surface reminiscent of the case of WTI. As prototype WTI, β-Bi$_4$X$_4$ offers a unique platform for exploring exotic physics with simple chemistry.

Band structures.— Both Bi$_4$I$_4$ and Bi$_4$Br$_4$ have stable α and β phases. The two phases crystallize in the same monoclinic space group C_{2h}^3 ($C2/m$), and differ only in the way their building blocks are stacked [20–23]. The α phases turn out to be normal insulators [24].
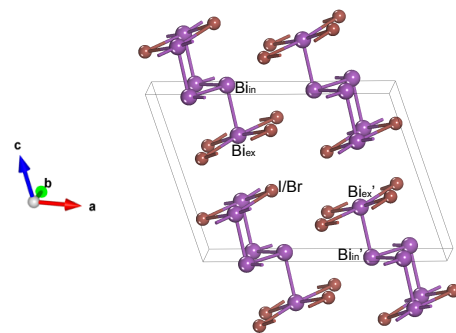

FIG. 1: The crystal structure of the conventional cell of β-Bi$_4$X$_4$ (X=I, Br). Bi$_{in}$ (Bi$_{ex}$) and Bi$'_{in}$ (Bi$'_{ex}$) atoms are interchanged under spacial inversion and invariant under (010) mirror reflection.
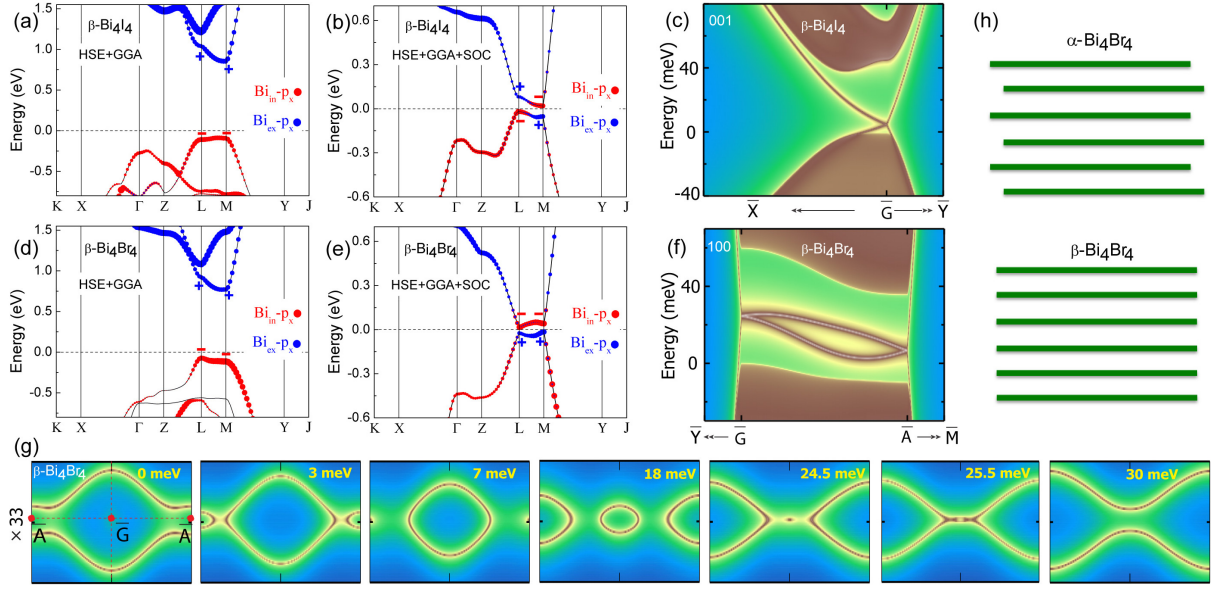
FIG. 2: (a)-(b) The bulk band structures for β-Bi$_4$I$_4$ without and with the SOC. The size of red (blue) dots indicates the weight of the relevant p_x orbital of Bi$_{in}$ (Bi$_{ex}$) atoms; the symbols $\pm$ label the parities of the bands at L and M points; the dashed lines are the Fermi levels. (c) The (001) cleave-surface states of β-Bi$_4$I$_4$. (d)-(e) The same as (a)-(b) but for β-Bi$_4$Br$_4$. (f) The (100) cleave-surface states of β-Bi$_4$Br$_4$ and (g) their Lifshitz transitions. Vertical dimensions in (g) are magnified by 33 times for clarity. (h) The illustration of the stacking orders in α- and β-Bi$_4$Br$_4$. The β (α) phase is a stack of single (double) (001) layers; each layer denoted by a green line is a QSHI.

As the β phases have rather similar lattice structures, by way of illustration we refer to β-Bi$_4$I$_4$ that has been experimentally synthesized, and the explicit lattice constants and atom positions of β-Bi$_4$Br$_4$ are given in Table S1 [24]. Figure 1a shows the conventional cell of β-Bi$_4$I$_4$, in which $a = 14.386$ Å, $b = 4.430$ Å, $c = 10.493$ Å, and $\beta = 107.87°$. One unit cell consists of four I atoms and four Bi atoms that can be divided into two types. The two internal Bi atoms, labeled as Bi$_{in}$ and Bi$'_{in}$, form zigzag atomic chains with the nearest neighbor distance of 3.04 Å. The two external Bi atoms, labeled as Bi$_{ex}$ and Bi$'_{ex}$, are each bonded to four I atoms with the Bi-I distance of 3.14 Å and to one internal Bi atom with a distance of 3.06 Å. The crystal has two independent symmetries, spatial inversion and mirror reflection. Under (010) mirror reflection, the four Bi atoms are invariant. Upon spatial inversion, the two Bi atoms are interchanged for each type. As suggested by Fig. 1a, β-Bi$_4$I$_4$ is a periodic stack of atomic chains aligned to the b direction. Indeed, we find that the interlayer binding energies for (100) and (001) planes are about 20 meV/Å^2, comparable to 12 meV/Å^2 for graphite [40] and 26 meV/Å^2 for MoS$_2$ [41]. Evidently, the β phases are van der Waals (vdW) materials, but with *two* cleavage surfaces.

We employ the HSE hybrid functional method [24], more accurate than GGA, to carry out our density functional theory (DFT) calculations of band structures. The vdW corrections [24] and the lattice relaxations are taken into account to optimize the crystal structures. The pro-

jected bands of β-Bi$_4$I$_4$ without and with spin-orbit couplings (SOC) are shown in Figs. 2a-2b, respectively. The bands near the gap are mainly contributed from the Bi p_x orbitals. Without SOC, the conduction and valence band edges at both L and M points are respectively from the Bi$_{ex}$ and Bi$_{in}$ orbitals, which are identified to exhibit opposite parities. When SOC are included, the constituents and parities of the conduction and valence bands remain the same at L, whereas they are inverted at M. Based on the parity criterion [25] β-Bi$_4$I$_4$ is a STI with $(1; 110)$ invariants and a 39 meV indirect gap. As plotted in Fig. 2c, we further obtain one surface Dirac cone at the (001) cleavage surface. Notably, the Dirac cone is highly anisotropic because the surface is parallel to the atomic chains.

We now study the band structure of β-Bi$_4$Br$_4$, which share evident similarities to that of β-Bi$_4$I$_4$. However, the band inversion occurs at both M and L points in β-Bi$_4$Br$_4$, as shown in Figs. 2d-2e. It follows [25] that β-Bi$_4$Br$_4$ is a WTI with $(0; 001)$ invariants and a 32 meV indirect gap. We further calculate the surface states for the two natural cleave surfaces, (100) and (001). The (001) surface are anticipated to host neither protected surface states nor dangling bond states, since M and L are projected into the same point. Our calculations verify this picture (not shown). In contrast, at the (100) surface, M and L are projected into two distinct points $\bar{G}$ and $\bar{A}$. As shown in Fig. 2f, our calculations identify the presence of two surface Dirac cones at $\bar{G}$ and $\bar{A}$ and

the absence of dangling bond states. The (100) surface states exhibit prominent anisotropy, for the aforementioned reason. Moreover, the two surface Dirac points are at different energies. These two features enrich the Fermi surface topology of the (100) surface states. Fig. 2g characterizes the four corresponding Lifshitz transitions, as we now explain in ascending energy. At zero energy, the two hole pockets around $\bar{G}$ and $\bar{A}$ are connected. As the energy increases, e.g., to 3 meV, the two pockets are disconnected after the first Lifshitz transition. At 7 meV, the second transition occurs; the hole pocket at $\bar{A}$ contracts into a Dirac point, followed by the emergence of an electron pocket. At higher energies, the disconnected electron and hole pockets coexist up to the third transition at about 24 meV, in which the hole pocket at $\bar{G}$ contracts into a Dirac point and then an electron pocket emerges. Ultimately, the fourth transition occurs and the two electron pockets become connected.

Interestingly, the STI β-Bi$_4$I$_4$ is also a topological crystalline insulator [26–28] whereas the WTI β-Bi$_4$Br$_4$ is not [24]. In sharp contrast to the case of β phase, both α-Bi$_4$I$_4$ and α-Bi$_4$Br$_4$ are normal insulators (NI) [24]. The contrasting topological properties of the α and β phases can be understood in the way illustrated by Fig. 2h. The β (α) phase is a stack of single (double) (001) layers. For Bi$_4$Br$_4$, the single (001) layer was demonstrated to be a QSHI with a 0.18 eV gap [41]. Given the weak interlayer couplings, the β phase is a WTI with similar band inversions at $k_z = 0$ and $k_z = \pi$ planes, whereas the α phase is trivial since each bilayer is a NI. For Bi$_4$I$_4$, the single (001) layer was shown to be close to the QSHI-NI critical point [41]. Thus, while the α phase is definitely a NI, the β phase is not necessarily a WTI, depending on the details. However, as we will show, β-Bi$_4$I$_4$ can become WTI under uniaxial strain.

Phase transitions.— We now construct an effective model for the β phases. The time-reversal-invariant M and L points have the little group C_{2h}^3 with two independent symmetries, spatial inversion $\mathcal{P} = \tau_z$ and mirror reflection $\mathcal{M}_y = i\sigma_y$. Here $\boldsymbol{\tau}$ and $\boldsymbol{\sigma}$ are the orbital and spin Pauli matrices. By convention we choose the time-reversal operator $\mathcal{T} = iK\sigma_y$ with K the complex conjugation. Given the three symmetries, to the linear order the $k \cdot p$ Hamiltonians near L and M may be written as

$$\mathcal{H}^i = v_x^i k_x \sigma_y \tau_x + v_y^i k_y \sigma_x \tau_x + v_z^i k_z \tau_y + m^i \tau_z + c^i, \quad (1)$$

where i refers to M or L, $\boldsymbol{v}$ are the velocities, c is the energy offset, and m is the energy gap with $m < 0$ denoting invertion. For β-Bi$_4$I$_4$ only m^M is negative; for β-Bi$_4$Br$_4$ both $m^{M/L}$ are negative.

With Eq. (1), we explore the strain effects on the β phases. The strain tensor ε_{ij} is rank-2 and invariant under time reversal. With these two facts and the original symmetries of $\mathcal{H}$, the strain induced perturbations to the
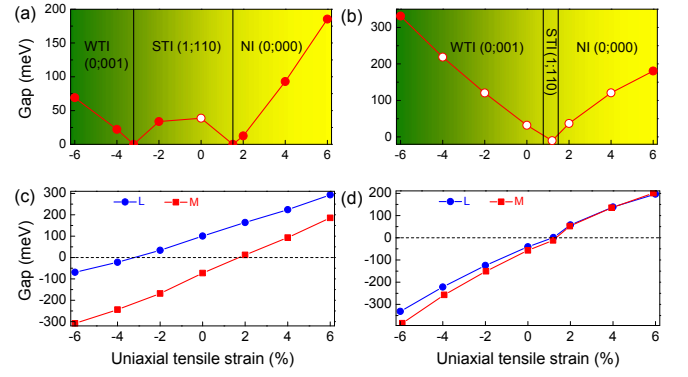

FIG. 3: The topological phase diagrams versus the uniaxial strain along the a axis are depicted in (a) for β-Bi$_4$I$_4$ and (b) for β-Bi$_4$Br$_4$. The corresponding direct gaps at L and M points are shown in (c) for β-Bi$_4$I$_4$ and (d) for β-Bi$_4$Br$_4$. A solid (open) dot denotes a direct (indirect) gap; the minus sign of a gap indicates a band inversion.

lowest order take the form of

$$\delta\mathcal{H}^i = \delta\mathcal{H}_0^i + \left(\varepsilon_{11}\lambda_{11}^i + \varepsilon_{22}\lambda_{22}^i + \varepsilon_{33}\lambda_{33}^i + \varepsilon_{13}\lambda_{13}^i\right)\tau_z, (2)$$

where λ_{ij} are deformation potentials, and $\delta\mathcal{H}_0^i$ is a rigid shift of all bands with a form similar to that in the parentheses. Clearly, applying strain along the $\boldsymbol{a}$, $\boldsymbol{b}$, or $\boldsymbol{c}$ axis would change the direct gaps and hence the band inversions at the M and L points. It follows that the topological phase transitions among NI, STI, and WTI can be tuned by the uniaxial strain.

This prediction can be verified by our DFT calculations [24] with strain along the $\boldsymbol{a}$ axis, as shown in Fig. 3. In this case, the deformation potentials at M and L points exhibit the same sign and similar magnitudes. For the STI β-Bi$_4$I$_4$, under more than 1.5% tensile strain, the inverted bands at M become un-inverted while those at L remain not inverted, yielding a STI to NI transition. On the other hand, under more than 3.3% compressive strain, the bands at L become inverted while those at M remain inverted, producing a STI to WTI transition. For the WTI β-Bi$_4$Br$_4$, the inverted gaps at L and M both increase with increasing the compressive strain, resulting a larger gap WTI. As the tensile strain increases, however, there are two successive transitions from the WTI to a STI and then to a NI, because the bands at L become un-inverted prior to those at M. Similar phase transitions can also be driven by strain along other axes [24]. These results are suggestive of a feasible way to engineer or stabilize the WTI phase.

Composite WSM.— Near the NI-STI transition, there emerges a WSM phase with only pairs of Weyl points [42–51] at Fermi energy, when $\mathcal{P}$ or $\mathcal{T}$ symmetry is broken. Each Weyl node is locally protected by the Chern number of a constant-energy surface enclosing it. One might naively think the same WSM phase emerges near the WTI-STI transition. In fact, the emergent phase turns
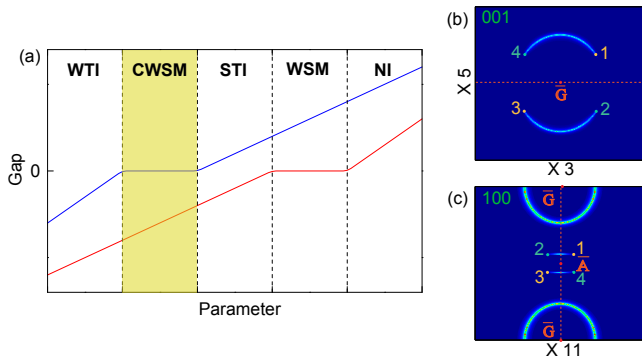
FIG. 4: (a) Schematic phase diagram of NI, STI, WSM, WTI, and the novel phase CWSM. The two curves depict the direct gaps near the relevant L and M points. (b) Existence of two open Fermi arcs at the (001) surface of the calculated CWSM. (c) Coexistence of two open Fermi arcs and one closed Fermi circle at the (100) surface of the same CWSM. In (b) and (c), the dimensions have been magnified for clarity.

out to be novel. We now examine such a phase using β-Bi_4I_4 under 3.3% compressive strain (see Fig. 3a). The $\mathcal{P}$ symmetry can be broken by a possible energy difference between the Bi and Bi$'$ atoms. Because of the low symmetry, only two pairs of Weyl points appear at the WTI-STI transition; the bulk is a standard WSM. At the (001) surface, there are two open Fermi arcs connecting the four projected Weyl nodes, as shown in Fig. 4b. At the (100) surface, surprisingly, there exists one closed Fermi circle in addition to the anticipated Fermi arcs, as shown in Fig. 4c. We dub this novel phase the *composite* WSM (CWSM). When $\mathcal{P}$ asymmetry is small, while the Weyl points emerge near L, the band gap remains inverted at M. As a consequence, there are surface states locally, separated by a large crystal momentum, at the (100) surface where L and M project into distinct points $\bar{A}$ and $\bar{G}$. In contrast, at the (001) surface where L and M project into the same point $\bar{G}$, the Fermi arcs appear attribute to the nontrivial Chern numbers, whereas the Fermi circle disappears because of its strong scattering with the metallic background. Intriguingly, the Fermi arcs generically appear at any surface like the case for WSM, whereas the Fermi circle only appears at selected surfaces like the case for WTI. Fundamentally, the most generic topological phase diagram should be modified to Fig. 4a, when $\mathcal{P}$ or $\mathcal{T}$ symmetry is broken, to include the novel CWSM phase near the WTI-STI transition.

Discussions.— As prototype WTI, β-Bi_4X_4 (X=I, Br) offer a new platform for exploring exotic physics with simple chemistry. In addition to the strain-induced topological phase transitions, CWSM phase, and the $\alpha-\beta$ domain wall, the two (100) surface states is particularly appealing, e.g., the spin texture, the Landau level crossing, and the exciton condensation triggered by the nesting of the electron and hole pockets. In the thin-film QSHI limit, the small velocity along the $\boldsymbol{a}$ or $\boldsymbol{c}$ axis can be uti-

lized to study the helical Luttinger liquid [52] and the $\mathcal{Z}_4$ parafermions [53–55]. As for the CWSM, physics can be enriched by single-particle couplings or many-body interactions between the open Fermi arcs and the closed Fermi circle.

WTI have been proved to be *strong* against disorder [56–58], as long as $\mathcal{U}(1)$, $\mathcal{T}$, and translational symmetries are respected on average. Breaking any symmetry at the (100) surface of β-Bi_4Br_4 or strained β-Bi_4I_4 may induce an exotic phenomenon. A topological defect, e.g., a screw dislocation [59] or a step edge [17, 60], can break a translational symmetry binding a helical edge modes. A Zeeman field can break $\mathcal{T}$ symmetry yielding a quantum anomalous Hall effect [61] with a Chern number from -2 to 2, tunable by the field orientation [28]. A proximity coupling to an $s_\pm$ wave (e.g., iron-based) superconductor can break $\mathcal{U}(1)$ gauge symmetry producing a $\mathcal{Z}_2$ topological superconductor with a Majorana Kramers pair [62].

* Electronic address: ygyao@bit.edu.cn
† Electronic address: zhang@utdallas.edu
[1] M. Z. Hasan, and C. L. Kane, Rev. Mod. Phys. **82**, 3045 (2010).
[2] X.-L. Qi and S.-C. Zhang, Rev. Mod. Phys. **83**, 1057 (2011).
[3] J. E. Moore, Nature **464**, 194 (2010).
[4] J. Alicea and A. Stern, Nobel Symposium: Phys. Scr. **T164** 014006 (2015).
[5] L. Fu, C. L. Kane, and E. J. Mele, Phys. Rev. Lett. **98**, 106803 (2007).
[6] J. E. Moore and L. Balents, Phys. Rev. B **75**, 121306 (2007).
[7] R. Roy, Phys. Rev. B **79**, 195322 (2009).
[8] Y. Xia, D. Qian, D. Hsieh, L. Wray, A. Pal, H. Lin, A. Bansil, D. Grauer, Y. S. Hor, R. J. Cava, and M. Z. Hasan, Nat. Phys. **5**, 398 (2009).
[9] Y. Chen, J. G. Analytis, J. Chu, Z. Liu, S. Mo, X. Qi, H. Zhang, D. Lu, X. Dai, Z. Fang, S. Zhang, I. R. Fisher, Z. Hussain, and Z. Shen, Science **325**, 178 (2009).
[10] M. Franz, Nat. Mat. **9**, 536 (2010).
[11] K. Yang, W. Setyawan, S. Wang, M. Nardelli, and S. Curtarolo, Nat. Mat. **11**, 614 (2012).
[12] B.-H. Yan and S.-C. Zhang, Rep. Prog. Phys. 75, 096501 (2012).
[13] Y. Ando, J. Phys. Soc. Jpn. 82, 102001 (2013).
[14] E. J. Mele, Nobel Symposium: Phys. Scr. **T164** 014004 (2015).
[15] B.-H. Yan, L. Müchler, and C. Felser, Phys. Rev. Lett. **109**, 116406 (2012).
[16] B. Rasche, A. Isaeva, M. Ruck, S. Borisenko, V. Zabolotnyy, B. Buchner, K. Koepernik, C. Ortix, M. Richter, and J. van den Brink, Nat. Mater. **12**, 422 (2013).
[17] C. Pauly, B. Rasche, K. Koepernik, M. Liebmann, M. Pratzer, M. Richter, J. Kellner, M. Eschbach, B. Kaufmann, L. Plucinski, C. M. Schneider, M. Ruck, J. van den Brink, and M. Morgenstern, Nat. Phys. **11**, 338 (2015).
[18] G. Yang, J. Liu, L. Fu, W. Duan, and C. Liu, Phys. Rev. B **89**, 085312 (2014).

[19] X. Li, F. Zhang, Q. Niu, and J. Feng, Sci. Rep. **4**, 6397 (2014).

[20] H. G. von Schnering, H. von Benda, and C. Kalveram, Z. Anorg. Allg. Chem. **438**, 37 (1978).

[21] H. von Benda, A. Simon, and W. Bauhofer, Z. Anorg. Allg. Chem. **438**, 53 (1978).

[22] E. V. Dikarev, B. A. Popovkin, A. V. Shevelkov, Russ. Chem. Bull. Int. Ed. **50**, 2304 (2001).

[23] T. G. Filatovaa, P. V. Gurinb, L. Klooc, V. A. Kulbachinskiib, A. N. Kuznetsova, V. G. Kytinb, M. Lindsjoc, and B. A. Popovkina, J. Solid State Chem. **180**, 1103 (2007).

[24] See Supplemental Material [url], which includes Refs. [20–23, 25–39].

[25] L. Fu and C. L. Kane, Phys. Rev. B **76**, 045302 (2007).

[26] T. H. Hsieh, H. Lin, J. Liu, W. Duan, A. Bansil, and L. Fu, Nat. Commun. 3, 982 (2012).

[27] J. C. Y. Teo, L. Fu, and C. L. Kane, Phys. Rev. B **78**, 045426 (2008).

[28] F. Zhang, X. Li, J. Feng, C. L. Kane, and E. J. Mele, arXiv:1309.7682 (2013).

[29] G. Kresse and J. Furthmüller, Phys. Rev. B **54**, 11169 (1996).

[30] J. P. Perdew, K. Burke, and M. Ernzerhof, Phys. Rev. Lett. **77**, 3865 (1996).

[31] G. Kresse and D. Joubert, Phys. Rev. B **59** 1758 (1999).

[32] J. Heyd, G. E. Scuseria, and M. J. Ernzerhof, Chem. Phys. **118**, 8207 (2003).

[33] A. Mostofi, J. R. Yates, Y.-S. Lee, I. Souza, D. Vanderbilt, and N. Marzari, Comput. Phys. Commun. **178**, 685 (2008).

[34] N. Marzari and D. Vanderbilt, Phys. Rev. B **56**, 12847 (1997).

[35] I. Souza, N. Marzari, and D. Vanderbilt, Phys. Rev. B **65**, 035109 (2001).

[36] M. P. L. Sancho, J. M. L. Sancho, and J. Rubio, J. Phys. F: Met. Phys. **15**, 851 (1985).

[37] M. Dion, H. Rydberg, E. Schroder, D. C. Langreth, and B. I. Lundqvist, Phys. Rev. Lett. **92**, 246401 (2004).

[38] J. Klimes, D. R. Bowler, and A. Michaelides, Phys. Rev. B **83**, 195131 (2011).

[39] A. Togo, F. Oba, and I. Tanaka, Phys. Rev. B **78**, 134106 (2008).

[40] Z. Liu, J. Z. Liu, Y. Cheng, Z. Li, L. Wang, and Q. Zheng, Phys. Rev. B **85**, 205418 (2012).

[41] J.-J. Zhou, W. Feng, C.-C. Liu, S. Guan, and Y. Yao, Nano Lett. **14**, 4767 (2014).

[42] G. E. Volovik, The Universe in a Helium Droplet (Clarendon Press, Oxford, 2003).

[43] S. Murakami, New J. Phys. **9**, 356 (2007).

[44] X. Wan, A. M. Turner, A. Vishwanath, and S. Y. Savrasov, Phys. Rev. B **83**, 205101 (2011).

[45] A. A. Burkov, and L. Balents, Phys. Rev. Lett. **107**, 127205 (2011).

[46] K.-Y. Yang, Y.-M. Lu, and Y. Ran, Phys. Rev. B **84**, 075129 (2011).

[47] C. Fang, M. J. Gilbert, X. Dai, and B. A. Bernevig, Phys. Rev. Lett. **108**, 266802 (2012).

[48] S. M. Young, S. Zaheer, J. C. Y. Teo, C. L. Kane, E. J. Mele, and A. M. Rappe, Phys. Rev. Lett. **108**, 140405 (2012).

[49] Z. Wang, Y. Sun, X.Q. Chen, C. Franchini, G. Xu, H. Weng, X. Dai, and Z. Fang, Phys. Rev. B **85**, 195320 (2012).

[50] S. A. Yang, H. Pan, and F. Zhang, Phys. Rev. Lett. **113**, 046401 (2014).

[51] B. J. Yang and N. Nagaosa, Nat. Commun., **5**, 4898 (2014).

[52] T. Li, P. Wang, H. Fu, L. Du, K. A. Schreiber, X. Mu, X. Liu, G. Sullivan, Gábor A. Csáthy, X. Lin, R. Du, Phys. Rev. Lett. **115** 136804 (2015).

[53] F. Zhang and C. L. Kane, Phys. Rev. Lett. **113**, 036401 (2014).

[54] C. P. Orth, R. P. Tiwari, T. Meng, and T. L. Schmidt, Phys. Rev. B **91**, 081406 (2015).

[55] D. F. Mross, A. Essin, J. Alicea, and A. Stern, arXiv:1507.01587 (2015).

[56] Z. Ringel, Y. E. Kraus, and A. Stern, Phys. Rev. B **86**, 045102 (2012).

[57] R. S. K. Mong, J. H. Bardarson, and J. E. Moore, Phys. Rev. Lett. **108**, 076804 (2012).

[58] L. Fu and C. L. Kane, Phys. Rev. Lett. **109**, 246605 (2012).

[59] Y. Ran, Y. Zhang, and A. Vishwanath, Nature Physics **5**, 298 (2009).

[60] J.-J. Zhou, W. Feng, G.-B. Liu, and Y. Yao, New J. Phys. **17**, 015004 (2015).

[61] C.-X. Liu, S.-C. Zhang, and X.-L. Qi, Ann. Rev. Cond. Mat. Phys., **7** (2016).

[62] F. Zhang, C. L. Kane, and E. J. Mele, Phys. Rev. Lett. **111**, 056402 (2013).